

Testing the local void solution to the Hubble tension using baryon acoustic oscillation measurements over the last twenty years

Indranil Banik^{1,2}[★] and Vasileios Kalaitzidis²

¹*Institute of Cosmology & Gravitation, University of Portsmouth, Dennis Sciama Building, Burnaby Road, Portsmouth PO1 3FX, UK*

²*Scottish Universities Physics Alliance, University of Saint Andrews, North Haugh, Saint Andrews, Fife, KY16 9SS, UK*

Accepted XXX. Received YYY; in original form ZZZ

ABSTRACT

A promising solution to the Hubble tension is a local void that is roughly 20% underdense out to 300 Mpc, as suggested by galaxy number counts in the near-infrared. Gravitationally driven outflows from this KBC void might inflate redshifts enough to solve the Hubble tension, a scenario explored in detail by Haslbauer et al. We obtain predictions for the baryon acoustic oscillation (BAO) observables in their best-fitting void models and a control model that assumes the homogeneous *Planck* cosmology. We compare these models against our compilation of available BAO measurements from the past twenty years. We find that the quality and quantity of available measurements are best using the isotropically averaged distance D_V . Taking its ratio with the expected value in the control model yields good agreement with unity at high redshift, but a discrepancy appears that systematically grows with decreasing redshift. Assuming independent uncertainties, the 41 considered D_V observations give a total χ^2 of 70.5 for the control void-free model, while the void models give only 44.8 – 46.7 depending on the density profile. This represents a reduction in overall tension from 3.0σ without a void to $1.0\sigma - 1.2\sigma$ in the void models. The χ^2 differences are smaller when considering measurements of the angular BAO scale or its redshift depth, but the void-free model provides the worst fit in all cases. Overall, our results suggest that recent hints of BAO observables deviating from expectations in the homogeneous *Planck* cosmology could indicate a local void, which was motivated by considerations unrelated to BAO data or the Hubble tension.

Key words: cosmological parameters – cosmology: theory – cosmology: observations – distance scale – large-scale structure of Universe – gravitation

1 INTRODUCTION

Much of our information about cosmology comes from the cosmic microwave background (CMB; Dicke et al. 1965; Penzias & Wilson 1965). Prior to its emission at redshift $z = 1090$, matter and radiation were tightly coupled because of the high Thomson scattering cross-section of free electrons – neutral atoms were not yet stable. Sound waves propagating in the plasma imprinted a characteristic pattern of anisotropies in the CMB, with fluctuations at particular angular scales having more power than at slightly smaller or larger scales (de Bernardis et al. 2000; Spergel et al. 2003, 2007). The first acoustic peak in the CMB corresponds to the largest scale with such a local maximum, which in this case is also the global maximum of the whole power spectrum. Its physical size is set by how far a sound wave travels through the coupled baryon-photon plasma in the ≈ 380 kyr between the Big Bang and recombination.

The very pronounced first acoustic peak in the CMB implies an excess clustering of matter at a particular scale. This should also be evident at late times in the large-scale matter distribution. A major advance in cosmology has been the reliable detection of precisely this baryon acoustic oscillation (BAO) feature in the large-scale

distribution of galaxies (Cole et al. 2005; Eisenstein et al. 2005). However, the effect is greatly diminished compared to the first peak in the CMB power spectrum. In the standard cosmological model known as Lambda-Cold Dark Matter (Λ CDM; Efstathiou, Sutherland & Maddox 1990; Ostriker & Steinhardt 1995), this is because baryons fell into the potential wells generated by the dominant CDM component, which lacked oscillatory features in its power spectrum because by definition it did not interact with radiation. Since most of the matter is CDM rather than baryons, the significant oscillations in the baryonic power spectrum at recombination were substantially damped at later times.

Although the BAO feature in the galaxy distribution is rather subtle compared to that in the CMB, observations of BAOs at late times do play a very important role in modern cosmology (for a review, see Chen et al. 2024). This is because the BAO corresponds to a size of about 150 comoving Mpc (cMpc), which is so large that the density fluctuations are rather small, putting them well into the ‘linear regime’ of structure formation. Consequently, although the power on the BAO scale has grown, there has not been much change to the overall shape of the power spectrum plotted with respect to comoving separation. As a result, the length scale of the BAO peak serves as a standard ruler with fixed comoving length r_d since shortly after recombination. The observed angular scale of the BAO ruler at some redshift tells us the comoving distance

[★] E-mail: indranil.banik@port.ac.uk (Indranil Banik); vk44@st-andrews.ac.uk (Vasileios Kalaitzidis)

to that redshift. We can also gain complementary information from the redshift depth of the BAO ruler, which corresponds to orienting it parallel to the line of sight rather than within the plane of the sky. We discuss the BAO observables in more detail in Section 2.1.

Measurements of the cosmic expansion history have become increasingly important in recent years because of the Hubble tension, a persistent discrepancy between estimates of H_0 from observations in the early versus late Universe (for a review, see [Di Valentino 2021](#)). Sometimes referred to as the Hubble constant despite its drastic variation with time, H_0 is the present value of the Hubble parameter $H \equiv \dot{a}/a$, where an overdot denotes a derivative with respect to time t since the Big Bang, 0 subscripts indicate present values, and a is the cosmic scale factor normalised to unity today. We can predict H_0 by calibrating the Λ CDM model parameters to the CMB power spectrum, which requires that $H_0 = H_0^{\text{Planck}} = 67.4 \pm 0.5 \text{ km s}^{-1} \text{ Mpc}^{-1}$ ([Planck Collaboration VI 2020](#); [Tristram et al. 2024](#)). It is also possible to obtain H_0 using a variety of other probes that do not rely on modelling the CMB power spectrum, for instance using the ages of the oldest stars and stellar populations in the Galactic disc and halo ([Cimatti & Moresco 2023](#); [Xiang et al. 2024](#)), or using the age difference between stellar populations at different z ([Cogato et al. 2024](#); [Guo et al. 2024](#)). The results are in good agreement with the *Planck* cosmology ([Banik & Samaras 2024](#)). This is non-trivial given the very narrow region of overlap between their considered non-CMB constraints in the space of H_0 and Ω_M , the present fraction of the cosmic critical density accounted for by matter.

We can also obtain H_0 from the local redshift gradient $z' \equiv dz/dr$, the rate at which the redshift of extragalactic objects increases with their distance r . In a homogeneously expanding universe, the redshift arises entirely from cosmological expansion over the light travel time r/c , in which case we must have that $H_0 = cz'$, where c is the speed of light (see equation 3 of [Mazurenko, Banik & Kroupa 2025](#)). The Universe does appear to be homogeneous and isotropic on Gpc scales, where the radio dipole is consistent with the expectation from the Solar velocity (known from the CMB dipole; [Planck Collaboration XXVII 2014](#)) causing sources ahead of the Sun to appear somewhat brighter, thus increasing the number of detectable sources in that direction (and vice versa; see [Wagenveld et al. 2024](#)). However, the local redshift gradient is usually measured on slightly smaller scales of a few hundred Mpc so that \dot{a} changes little over the corresponding range of lookback times (a typical choice is to use $z = 0.023 - 0.15$ and treat $a(t)$ as a parabola; see [Camarena & Marra 2020a,b](#)). The measured $cz' = 73.0 \pm 1.0 \text{ km s}^{-1} \text{ Mpc}^{-1}$ ([Riess et al. 2022](#)). This unexpectedly high local cz' is evident in a wide variety of studies that measure extragalactic distances using different instruments and techniques, some of which rely on Type Ia supernovae (SNe) while others do not ([Scolnic & Vincenzi 2023](#), and references therein). Distances obtained by the *James Webb Space Telescope* are in good agreement with those obtained previously by the *Hubble Space Telescope* ([Freedman et al. 2024](#); [Riess et al. 2024](#)). Observations of the fundamental plane (FP) relation of elliptical galaxies have recently anchored cz' to d_{Coma} , the distance to the Coma Cluster ([Said et al. 2024](#)). The FP-based cz' is in agreement with the other measurements if we adopt the typically reported $d_{\text{Coma}} \approx 100 \text{ Mpc}$, but $cz' = H_0^{\text{Planck}}$ only if $d_{\text{Coma}} > 110 \text{ Mpc}$, which exceeds any published measurement since 1990 ([Scolnic et al. 2025](#), and references therein).

A variety of solutions have been proposed for the Hubble tension ([Di Valentino et al. 2021](#), and references therein). Solutions that modify the physics prior to recombination are disfavoured for several reasons ([Vagnozzi 2023](#)), including the age issue mentioned

above (see also section 7.5 of [Poulin et al. 2023](#)). This can be avoided if the expansion history is altered slightly at late times so that \dot{a} is currently about 9% higher than in the *Planck* cosmology ([Harko 2023](#); [Yao & Meng 2023](#); [Rezazadeh et al. 2024](#)). The required more rapid acceleration of the expansion rate at late times implies an effective phantom equation of state for dark energy ([Dahmani et al. 2023](#)), which may be problematic ([Ludwick 2017](#)).

These difficulties motivate us to reconsider the assumption that $cz' = \dot{a}$, which is at the heart of the Hubble tension. Standard physics provides two main non-cosmological sources of redshift: peculiar velocity and gravitational redshift (GR). This raises the possibility that the anomalously high local cz' arises from our location within a large and deep void, outflows from which would create extra redshift. Moreover, if we were located close to the void centre, we would be on a potential hill, creating GR contributions to the redshift. Cosmic variance in the local cz' is only $0.9 \text{ km s}^{-1} \text{ Mpc}^{-1}$ in Λ CDM ([Camarena & Marra 2018](#)), but it is possible that structure formation is more efficient on scales $\gtrsim 100 \text{ Mpc}$. This scenario was considered in some detail by [Haslbauer, Banik & Kroupa 2020](#) (hereafter [HBK20](#)), who considered a simple model of spherically symmetric outflow from a void plus a systemic velocity of the whole void. Those authors evolved voids with three different initial underdensity profiles (Exponential, Gaussian, and Maxwell-Boltzmann) in a background *Planck* cosmology starting from $z = 9$. To enhance the growth of structure, they used a force law based on Milgromian dynamics (MOND; [Milgrom 1983](#); [Famaey & McGaugh 2012](#); [Banik & Zhao 2022](#)).

A local void introduces additional contributions to the redshift. In particular, equation 52 of [HBK20](#) shows that the observed redshift z satisfies:

$$1 + z = \frac{1}{a(t)} \sqrt{\frac{c + v_{\text{int}}}{c - v_{\text{int}}}} \exp\left(\frac{1}{c^2} \int g_{\text{void}} dr\right), \quad (1)$$

where a was the cosmic scale factor at the emission time t of an observed photon, g_{void} is the outward gravitational field induced by the void due to it having less density than the cosmic mean, and v_{int} is the outflow velocity in the reference frame of the void, which may be moving as a whole. However, the effect of any such systemic velocity would cancel out if observing sources at the same z over a wide range of sky directions, so we do not consider the void's systemic velocity further and deal only with v_{int} . For similar reasons, we also neglect our slight offset from the void centre. These assumptions were also made by [Mazurenko, Banik & Kroupa \(2025\)](#) when assessing how quickly the apparent cosmology returns to the *Planck* cosmology at high redshift, which is inevitable in any local or late-time solution to the Hubble tension. We note that when dealing with observations at very low $z \lesssim 0.05$, we cannot neglect either the systemic velocity of the void or our offset with respect to its centre. Therefore, both of these were carefully considered by [Mazurenko et al. \(2024\)](#) when comparing the velocity field in the void model against the observed bulk flow curve ([Watkins et al. 2023](#)), which measures the average velocity of galaxies within concentric spheres centred on our location ([Nusser 2016](#); [Peery, Watkins & Feldman 2018](#)).

Galaxy number counts in the near-infrared do indeed reveal a significant underdensity known as the KBC void ([Keenan, Barger & Cowie 2013](#)). This is an underdense region on a scale of around 300 Mpc (see their figure 11 and figure 1 of [Kroupa 2015](#)). The void is evident at optical ([Maddox et al. 1990](#); [Shanks 1990](#)), infrared ([Huang et al. 1997](#); [Busswell et al. 2004](#); [Frith et al. 2003](#),

2005, 2006; Keenan et al. 2013; Whitbourn & Shanks 2014, 2016; Wong et al. 2022), X-ray (Böhringer et al. 2015, 2020), and radio wavelengths (Rubart & Schwarz 2013; Rubart, Bacon & Schwarz 2014). The observed density contrast of the KBC void implies that it would raise the local cz' by about $11 \pm 2\%$, suggesting that the observed local cz' is quite consistent with $\dot{a} = H_0^{\text{Planck}}$ (see equation 5 of HBK20). Those authors also found that the void is in 6.04σ tension with the Λ CDM model based on a comparison with results from the Millennium XXL simulation (MXXL; Angulo et al. 2012). The analysis of HBK20 indicates that the KBC void is roughly 20% underdense out to 300 Mpc, but the apparent density contrast is roughly doubled by outflows induced by the void distorting the relation between distance and redshift compared to a homogeneous universe. This causes observers to overestimate their sampled volume when taking data out to some fixed redshift, causing them to find fewer galaxies than they are expecting. The apparent underdensity is $46 \pm 6\%$ without correcting for this effect, as shown by the light blue point on figure 11 of Keenan, Barger & Cowie (2013). A somewhat smaller apparent density contrast was claimed by Wong et al. (2022), but their figure 1b shows that the comoving luminosity density is still rising by $z = 0.08$, where their measurements stop. This corresponds to about 350 Mpc on figure 11 of Keenan, Barger & Cowie (2013), which shows that the luminosity density is nearly flat beyond this point out to the most distant measurements at around 800 Mpc. Therefore, the results in figure 1 of Wong et al. (2022) should be renormalised to the luminosity density at their last measured point, which is far more representative of the cosmic average. This would cause all their plotted luminosity densities to be scaled down by a factor of $2/3$. With this adjustment, their reported average density within the void of $0.8\times$ the cosmic mean would become only $0.53\times$ the cosmic mean, almost exactly in line with Keenan, Barger & Cowie (2013). This highlights the issue that observations with limited depth can underestimate the depth of a local void if they cannot adequately probe beyond it, which is required to correctly normalise the results.

The velocity field predicted by the local supervoid solution to the Hubble tension was further explored by Mazurenko et al. (2024) using the predicted bulk flow, the average velocity within some radius centred on our location. If we place ourselves at some locations in the proposed void, it is possible to obtain a good match to the observed bulk flow curve (Watkins et al. 2023), which is based on the CosmicFlows-4 catalogue of galaxy redshifts and redshift-independent distances obtained using various scaling laws (Tully et al. 2023a). On their largest probed scale of $250 h^{-1}$ Mpc (where $h \approx 0.7$ is the value of H_0 in units of $100 \text{ km s}^{-1} \text{ Mpc}^{-1}$), the observed bulk flows are quadruple the Λ CDM expectation and thus in $> 5\sigma$ tension with it (see figure 8 of Watkins et al. 2023). It was later found that their reported bulk flows are in ‘‘excellent agreement’’ with those found by Whitford, Howlett & Davis (2023) out to $173 h^{-1}$ Mpc, the outer limit to their more conservative analysis.

In this contribution, we test the local void model using a compilation of BAO measurements collected over the last twenty years. Outflow from a local void and GR due to our location on a potential hill inflate the redshift to any fixed distance, slightly distorting the relation between redshift and the BAO observables (Section 2.2). We predict these observables for three different initial void underdensity profiles (Exponential, Gaussian, and Maxwell-Boltzmann) using the best-fitting parameters for each profile as published in HBK20. Those authors mainly constrained the void parameters using the local cz' from SNe and the density profile of the KBC void, while fixing the background expansion history

to the *Planck* cosmology to ensure consistency with the CMB. Importantly, they did not consider BAO data, much of which was in any case not available at that time. This allows BAO observations to provide an independent test of their model.

As part of this test, we can also address whether a local void might be responsible for hints that recent BAO observations with the Dark Energy Spectroscopic Instrument (DESI; DESI Collaboration 2016, 2022) deviate from expectations in the homogeneous *Planck* cosmology (DESI Collaboration 2024). These hints for an anomaly primarily come from two redshift bins, so one has to exclude a significant amount of data to remove the hints (Wang et al. 2024). Moreover, there were indications from BAO measurements prior to DESI that $H(z)$ rises above expectations in the *Planck* cosmology at low z (Gómez-Valent et al. 2024). The DESI anomaly has been interpreted as indicating time variation of the dark energy density (Giarè et al. 2024; Wang et al. 2024), but we explore if it might instead be due to a local void.

After explaining our methods in Section 2, we present our results in Section 3 and discuss them in Section 4. We then conclude in Section 5. We use D_c to denote the comoving distance, which some studies call D_M .

2 METHODS

We explain how the BAO observables should be determined in a homogeneous cosmology (Section 2.1), for which we adopt the parameters $H_0 = 67.4 \text{ km s}^{-1} \text{ Mpc}^{-1}$ and $\Omega_M = 0.315$ (Planck Collaboration VI 2020). These values were adopted by HBK20, with a recent reanalysis of *Planck* data barely affecting the results (Tristram et al. 2024). We then discuss how the above predictions for the BAO observables should be revised to account for a local void (Section 2.2). We compare the homogeneous and local void models using a compilation of BAO observations over the last twenty years, which we discuss in Section 2.3.

2.1 The BAO observables in a homogeneous cosmology

Since the BAO feature is a 3D structure, we can detect it in the correlation function of galaxies both within the plane of the sky and along the line of sight. The transverse BAO signal appears as an excess at a particular angular scale

$$\Delta\theta = \frac{rd}{D_c}, \quad (2)$$

where D_c is the comoving distance to the effective redshift of the galaxies used to measure the BAO signal. D_c can be found from the underlying expansion history $a(t)$ using

$$D_c = \int_t^{t_0} \frac{c dt'}{a(t')} = \int_0^z \frac{c dz'}{H(z')}, \quad (3)$$

where t is the time since the Big Bang when the galaxies are observed, t_0 is the present epoch, and $z = a^{-1} - 1$ is the redshift. Note that if we were to calculate $\Delta\theta$ using instead the physical ruler size ar_d , we would get this in the numerator of Equation 2, but we would also need to use the angular diameter distance $D_A = aD_c$ in the denominator, causing the factors of a to cancel.

The parallel BAO signal appears as excess power at a particular difference between the redshifts of galaxies within the considered shell. The redshift depth of the BAO ruler is

$$\Delta z = \frac{rd}{D_H} = \frac{rdH(z)}{c}, \quad (4)$$

with the comoving Hubble distance $D_H \equiv c/H$ at any z . It will be helpful to think of Δz as arising from the different amounts of cosmic expansion over the different light travel times from the near and far ends of the BAO ruler, orienting it parallel to the line of sight.

2.2 Predicting the BAO observables from within a local void

A local void introduces additional non-cosmological contributions to the redshift (Equation 1). As a result, the integral with respect to z in Equation 3 must be understood as an integral with respect to the purely cosmological contribution to the redshift, which is

$$z_c \equiv a^{-1} - 1. \quad (5)$$

A local void does not affect Equation 2, but the additional non-cosmological redshift distorts the relation between D_c and z by raising the latter. This changes the predicted $\Delta\theta(z)$.

We obtain the predicted BAO observables in the local void models considered by HBK20 using the techniques discussed below. Those authors evolved a small initial underdensity forwards from $z = 9$ until the present time assuming three different initial underdensity profiles: Exponential, Gaussian, and Maxwell-Boltzmann. In each case, the authors found best-fitting void parameters (size, depth, and external field strength) by comparing to a variety of observations, including especially the observed density profile of the KBC void and the local cz' . In this contribution, we consider only their best-fitting parameters for each void profile.

Since the available BAO measurements (Section 2.3) are generally quite far out, we approximate that we are located at the void centre. This is justified by the finding that we should be $\lesssim 150$ Mpc from the void centre to match the observed bulk flow curve, with the best match requiring an even smaller distance (Mazurenko et al. 2024). This allows us to simplify our analysis substantially. However, the large redshifts of BAO measurements also force us to relax their assumption that light travel times are negligible, requiring us to consider our past lightcone in greater detail (Equation 6).

2.2.1 Angular scale

We begin by finding the predicted $D_c(a)$ in the homogeneous *Planck* cosmology with parameters $H_0 = 67.4 \text{ km s}^{-1} \text{ Mpc}^{-1}$ and $\Omega_M = 0.315$ (Planck Collaboration VI 2020) as these were the parameters adopted by HBK20. We note that the parameters have been updated only slightly in the final *Planck* data release (Tristram et al. 2024).

Similarly to HBK20, we consider a grid of particle trajectories with uniform spacing in their initial separation from the void centre. We find the intersection of each trajectory with our past lightcone using the same approach as in their section 3.3.3, which requires us to solve

$$r_c(t) = \int_t^{t_0} \frac{c dt'}{a(t')}, \quad (6)$$

where r_c is the comoving distance of the particle from the void centre, t is the time at which we observe the particle, and t_0 is the present time. We solve this for t using the Newton-Raphson method (using also information on the particle velocity) and record both a and z at that time, which we find using equations 45 and 52 of HBK20, respectively. We then find D_c by interpolating to the desired a using our previously found $D_c(a)$ assuming homogeneity (Equation 3), which tells us the comoving distance to the particle at time t . By repeating this procedure for all considered test particles,

we obtain the predicted $D_c(z)$. We also find the corresponding prediction without any local void by writing $D_c(a)$ as $D_c(z_c)$ using Equation 5 and assuming that $z = z_c$.

Since the BAO angular scale (Equation 2) varies hugely with z , it is common to divide $\Delta\theta$ by that in some fiducial cosmology to obtain the parameter

$$\alpha_\perp \equiv \frac{D_c}{r_d} \div \frac{D_c}{r_d} \Big|_{\text{fid}}, \quad (7)$$

where ‘fid’ subscripts indicate values calculated at the same z in the fiducial cosmology. In our case, this is the homogeneous *Planck* cosmology, which gives $r_d = 147.05 \pm 0.30 \text{ cMpc}$ (section 5.4 of Planck Collaboration VI 2020). Since the uncertainty in r_d is very small, we often discuss our results as if α_\perp measures D_c divided by its fiducial value at the same z .

2.2.2 Redshift depth

The impact on Δz must be found by considering the redshifts of photons emitted from the near and far ends of the BAO ruler. The difference arises from three main effects:

- (i) Cosmological expansion over the light travel time across the BAO ruler;
- (ii) Peculiar velocity variations within the void; and
- (iii) Evolution of the void over the light travel time.

To obtain the redshift depth of the BAO ruler at redshift z , we start from the comoving distance $D_{c,0}$ predicted by the void model at that z , including the non-cosmological contributions to z (Equation 1). We then quantify the redshifts z_\pm at which $D_c = D_{c,0} \pm r_d$. We find z_\pm using the Newton-Raphson algorithm, applying the secant method as it is difficult to analytically quantify the gradient. We then set

$$\Delta z = \frac{z_+ - z_-}{2}, \quad (8)$$

which we use to calculate D_H/r_d via Equation 4. We use this centred differencing approach to make our results more accurate. We repeat our calculations including only the cosmological contribution to z (Equation 5) to get the results without a local void.

Similarly to Equation 7, the redshift depth of the BAO ruler is usually normalised to its value in some fiducial cosmology by defining

$$\alpha_\parallel \equiv \frac{D_H}{r_d} \div \frac{D_H}{r_d} \Big|_{\text{fid}}. \quad (9)$$

Since the uncertainty in the *Planck* r_d is very small, we often discuss our results as if α_\parallel measures D_H divided by its fiducial value at the same z .

2.2.3 The Alcock-Paczynski (AP) test

Although there is very little uncertainty in the *Planck* value of r_d , this is reliant on theoretical assumptions concerning the early Universe. In principle, BAO measurements can provide useful cosmological constraints without assuming any particular value for r_d as long as we make the much less strict assumption that r_d has remained constant with time, a technique known as uncalibrated cosmic standards (UCS; Lin, Chen & Mack 2021).

Altering r_d would scale both α_\parallel and α_\perp by the same factor. This motivates us to consider their ratio, which is known as the AP

parameter α_{AP} (Alcock & Paczynski 1979):

$$\alpha_{\text{AP}} \equiv \frac{\alpha_{\perp}}{\alpha_{\parallel}}. \quad (10)$$

This cancels out the effect of possible issues with the fiducial r_d , so that $\alpha_{\text{AP}} \neq 1$ (a failure of the AP test) cannot be explained merely by altering r_d if we assume homogeneity. Instead, we would have to modify the shape of the expansion history. For this reason, the AP test was originally proposed as a way to detect dark energy. A major drawback of α_{AP} is that obtaining it observationally requires the ratio between two quantities each with their own uncertainty, making it less accurate.

2.2.4 Isotropic average

Though we have only discussed the BAO feature within the plane of the sky and along the line of sight, it is actually a 3D feature. The volume of this feature can be computed using the BAO observables, with the cube root of this volume then providing an isotropically averaged estimate of the size of the BAO ruler. This consideration has motivated the introduction of the derived BAO observable D_V (Eisenstein et al. 2005), which is defined as follows (see equation 2.6 of DESI Collaboration 2024):

$$D_V \equiv \left(z D_c^2 D_H \right)^{1/3}. \quad (11)$$

Similarly to the definitions of α_{\perp} and α_{\parallel} , it is common to divide D_V by its predicted value in some fiducial cosmology at the same z , which cancels out the factor of z in Equation 11. The ratio of D_V to its fiducial value is thus

$$\alpha_{\circ} = \left(\alpha_{\perp}^2 \alpha_{\parallel} \right)^{1/3}, \quad (12)$$

where the circle subscript indicates an isotropically averaged value. A major advantage of α_{\circ} is that since it is basically the geometric mean of α_{\perp} and α_{\parallel} (with the former counted twice), uncertainties are reduced for much the same reason that the average of two measurements is more accurate than either measurement on its own. This allows observers to report D_V even if the results are too inaccurate to report D_c and D_H individually.

2.3 The BAO sample

We test the local void scenario using a compilation of published BAO results from the last twenty years. These studies are summarised in Table 1, sorted in ascending order of redshift. Many studies are listed multiple times because they contribute results at different redshifts. At each redshift, we indicate which distance measures were published in that study.

In cases where D_c and D_H are both available, we can calculate D_V using Equation 11. We sometimes do so, but if possible, we use instead the published value of D_V and its uncertainty. If we have to work out the uncertainty ourselves, we assume independent errors on D_c and D_H given that these refer to orthogonal directions. We then combine their fractional errors in quadrature to obtain the fractional error on D_V .

$$\frac{\sigma(D_V)}{D_V} = \sqrt{\left[\frac{2}{3} \frac{\sigma(D_c)}{D_c} \right]^2 + \left[\frac{1}{3} \frac{\sigma(D_H)}{D_H} \right]^2}, \quad (13)$$

where $\sigma(x)$ is the uncertainty on any quantity x . We indicate which measurements of D_V were obtained in this way and which can be read off from the cited publication.

We work out the AP parameter in cases where we have both D_c and D_H . To get the uncertainty in α_{AP} , we again assume that D_c and D_H have independent fractional uncertainties, which we simply add in quadrature to obtain the fractional uncertainty in α_{AP} . This is similar to Equation 13, but with the factors of 1/3 and 2/3 both replaced by 1.

Although the BAO observable is a dimensionless ratio of some distance measure with r_d , some studies give the distance measure in Mpc, assuming a particular value for r_d . More modern studies are generally careful to avoid making this model-dependent assumption when publishing observations, but some older studies suffer from this issue. Fortunately, such studies generally state their assumed r_d , which we indicate in Table 1. In some cases, the assumed value of r_d is not mentioned in the study, but r_d can be obtained through the studies it cites. In these cases, we indicate the assumed r_d and also add a citation, since this does not follow directly from the study giving the BAO measurement. In a very small number of cases, several studies are cited in relation to the assumed r_d , making it unclear exactly what value was assumed when reporting the BAO distance measure in Mpc. In these cases, the cited studies all give numerically very similar values of r_d , so we pick whichever one we thought was most suitable. We caution that older studies that list a BAO distance measure in Mpc often assume a slightly different r_d to the modern estimate of 147 cMpc because they predate the *Planck* mission, forcing them to make do with older CMB observations, generally from the Wilkinson Microwave Anisotropy Probe (WMAP; Bennett et al. 2003; Hinshaw et al. 2003; Spergel et al. 2003). Comparison of these older studies with a CMB-derived cosmology should be redone in the *Planck* era with updated r_d . This can be calculated using equation 6 of Eisenstein & Hu (1998), with equation 12 of Percival et al. (2010) providing an expansion about the WMAP five-year parameters (Komatsu et al. 2009).

3 RESULTS

We begin by presenting results on D_c , which is inversely related to the BAO angular scale $\Delta\theta$ (Equation 2). Our results are shown in Figure 1 in terms of the parameter α_{\perp} (Equation 7). By definition, the expectation in the homogeneous *Planck* cosmology is 1 at all z , though there is a small 0.2% uncertainty equal to the fractional uncertainty on the *Planck* r_d , which we show as a grey band. The coloured solid lines show results from the three void profiles considered by HBK20, with the best-fitting void parameters from their study used in each case. These parameters were obtained without regard to BAO results, many of which were not available at that time. All three models have $\alpha_{\perp} \rightarrow 1$ at high z because the effect of a local void decays beyond it (see also Mazurenko, Banik & Kroupa 2025). At low z , these models reach $\alpha_{\perp} \approx 0.9$ because the models were constrained to solve the Hubble tension, implying that $cz' \approx 1.1 H_0^{\text{Planck}}$. This means that in the local universe, the distance to any fixed redshift is about 10% smaller than in the homogeneous *Planck* cosmology. Since the void models were constrained using the observed density profile of the KBC void (Keenan, Barger & Cowie 2013), they all converge to unity at high z at a similar rate. This makes it difficult to distinguish the models from each other. We also show results without the GR contribution using dashed lines, helping to show its impact by comparison with solid lines in the same colour. At large redshift, there is negligible outflow velocity due to a local void, making the GR contribution mainly responsible for the predicted deviations from $\alpha_{\perp} = 1$. This behaviour is also evident in figure 3 of Mazurenko, Banik & Kroupa (2025).

Table 1. Our compilation of available BAO measurements from the indicated survey and reference, sorted in ascending order of redshift. Each symbol in columns 4 – 7 indicates that the cited study was used to obtain the BAO observable given in the column heading. Circle symbols indicate that we used the published value, while diamond symbols indicate that we calculated the BAO observable using the information provided. Black symbols indicate values used in our χ^2 calculation (Section 3.1), while grey symbols indicate values not used there. This occurs if the results were later reanalysed and used for a different data point, or if results are available using both coarser and finer redshift bins, in which case we plot the former to avoid crowding but use the latter for χ^2 to extend the redshift range. We provide brief comments where necessary in the final column.

z	Survey	Reference	D_C	D_H	α_{AP}	D_V	Notes
0.068	Ho'oleilana	Tully et al. (2023b)				●	α_c from individual structure at $z = 0.068^{+0.003}_{-0.007}$
0.097	6dFGS	Carter et al. (2018)				●	$r_d = 147.5$ cMpc
0.106	6dFGS	Beutler et al. (2011)				●	
0.11	SDSS DR17	de Carvalho et al. (2021)	●				
0.122	SDSS + 6dFGS	Carter et al. (2018)				●	$r_d = 147.5$ cMpc
0.15	SDSS DR7	Ross et al. (2015)				●	$r_d = 148.69$ cMpc
0.2	SDSS + 2dFGRS	Percival et al. (2007)				●	
0.2	SDSS DR7	Percival et al. (2010)				●	
0.24	SDSS DR12	Chuang et al. (2017)	●	●	◆	●	$r_d = 147.66$ cMpc; finer redshift bin
0.295	DESI DR1	DESI Collaboration (2024)				●	
0.32	SDSS DR9	Anderson et al. (2014)				●	$r_d = 149.28$ cMpc
0.32	SDSS DR12	Alam et al. (2017)	●	●	◆	◆	
0.32	SDSS DR12	Chuang et al. (2017)	●	●	◆	●	Coarser redshift bin
0.35	SDSS DR5	Percival et al. (2007)				●	
0.35	SDSS DR7	Percival et al. (2010)				●	
0.35	SDSS DR7	Chuang, Wang & Hemantha (2012)				●	
0.35	SDSS DR7	Chuang & Wang (2012)				●	
0.37	SDSS DR12	Chuang et al. (2017)	●	●	◆	●	Finer redshift bin
0.38	SDSS DR12	Alam et al. (2017)	●	●	◆	◆	$r_d = 147.78$ cMpc
0.38	SDSS DR12	Ivanov et al. (2020)	●	●	◆	◆	$r_d = 147.09$ cMpc
0.38	SDSS DR12	Schirra, Quartin & Amendola (2024)	●	●	◆	●	
0.44	WiggleZ Final DR	Blake et al. (2012)	●	●	◆	●	
0.49	SDSS DR12	Chuang et al. (2017)	●	●	◆	●	Finer redshift bin
0.51	SDSS DR12	Alam et al. (2017)	●	●	◆	◆	
0.51	DESI DR1	DESI Collaboration (2024)	●	●	◆	◆	
0.54	SDSS DR8	Seo et al. (2012)	●				
0.57	SDSS DR12	Alam et al. (2017)	●	●	◆	◆	$r_d = 147.78$ cMpc
0.57	SDSS DR12	Slepian et al. (2017)				●	$r_d = 147.66$ cMpc
0.59	SDSS DR12	Chuang et al. (2017)	●	●	◆	◆	Coarser redshift bin
0.6	WiggleZ Final DR	Blake et al. (2012)	●	●	◆	◆	$r_d = 153.3$ cMpc (Blake et al. 2011)
0.61	SDSS DR12	Alam et al. (2017)	●	●	◆	●	$r_d = 147.78$ cMpc
0.61	SDSS DR12	Ivanov et al. (2020)	●	●	◆	◆	$r_d = 147.09$ cMpc
0.61	SDSS DR12	Schirra et al. (2024)	●	●	◆	●	
0.64	SDSS DR12	Chuang et al. (2017)	●	●	◆	●	Finer redshift bin
0.7	DECaLS DR8	Sridhar et al. (2020)	●				$r_d = 147.05$ cMpc (Planck Collaboration VI 2020)
0.7	SDSS DR16	Gil-Marín et al. (2020)	●	●	◆	◆	
0.7	SDSS DR16	Zhao et al. (2021)	●	●	◆	◆	Results identical to 2020 preprint
0.706	DESI DR1	DESI Collaboration (2024)	●	●	◆	◆	
0.73	WiggleZ Final DR	Blake et al. (2011)				●	
0.73	WiggleZ Final DR	Blake et al. (2012)	●	●	◆	◆	$r_d = 153.3$ cMpc (Blake et al. 2011)
0.77	SDSS DR16	Wang et al. (2020)	●	●	◆	◆	
0.8	SDSS DR14	Zhu et al. (2018)	●	●	◆	◆	$r_d = 147.18$ cMpc (Planck Collaboration VI 2020)
0.81	DES Y1	DES Collaboration (2019)	●				
0.835	DES Y3	DES Collaboration (2022)	●				
0.85	SDSS DR16	de Mattia et al. (2021)				●	
0.85	DES Y6	DES Collaboration (2024)	●				
0.874	DECaLS DR8	Sridhar et al. (2020)	●				$r_d = 147.05$ cMpc (Planck Collaboration VI 2020)
0.93	DESI DR1	DESI Collaboration (2024)	●	●	◆	◆	
1.317	DESI DR1	DESI Collaboration (2024)	●	●	◆	◆	
1.48	SDSS DR16	Neveux et al. (2020)	●	●	◆	◆	Consensus BAO results (see also Hou et al. 2021)
1.491	DESI DR1	DESI Collaboration (2024)				●	
2.33	DESI DR1	DESI Collaboration (2024)	●	●	◆	◆	
2.33	DESI + SDSS	DESI Collaboration (2024)	●	●	◆	◆	
2.33	SDSS DR16	du Mas des Bourboux et al. (2020)	●	●	◆	◆	
2.4	DES Y1	DES & SPT Collaborations (2018)	●	●	◆	◆	

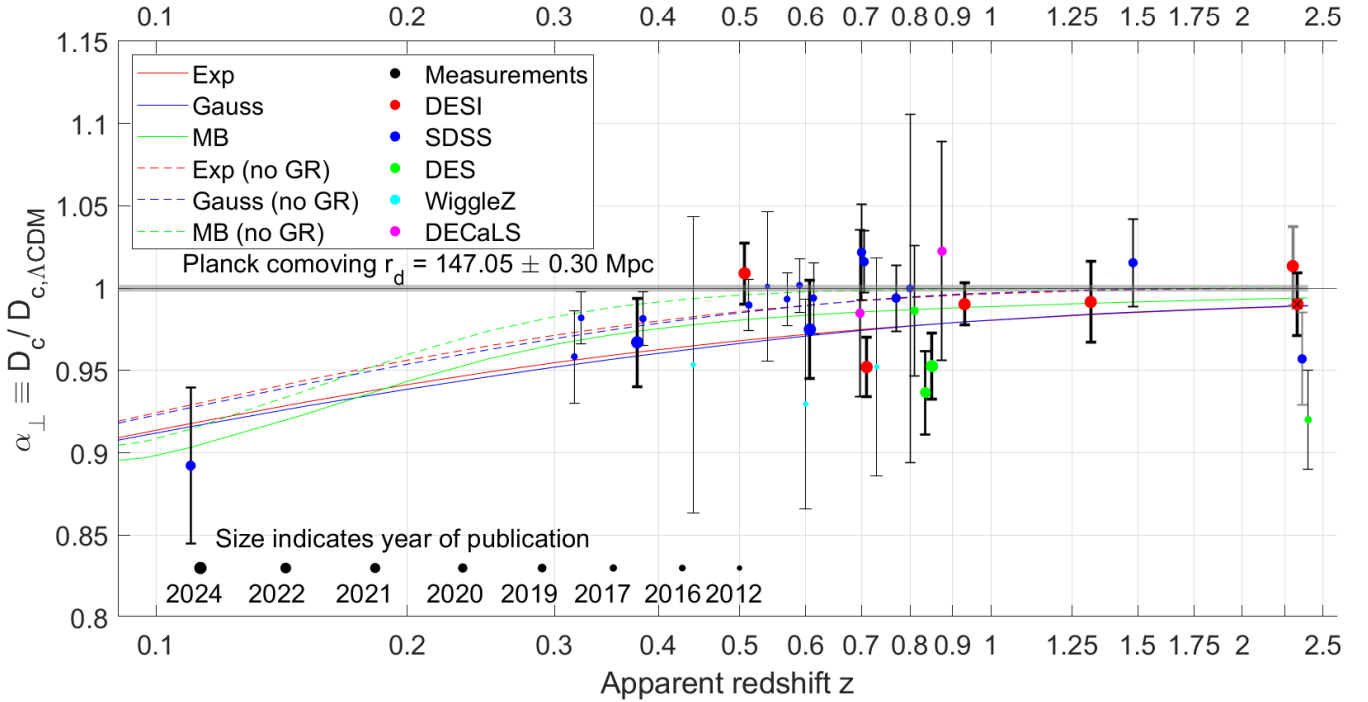


Figure 1. The ratio α_{\perp} (Equation 7) of the comoving distance D_c to the Λ CDM expectation at the same redshift as a function of the apparent redshift z , both according to the model (solid lines) and observations (points with uncertainties). Different void profiles are shown in different colours, as indicated in the legend. The dashed lines show results neglecting the GR contribution (Equation 1). The observations used here are indicated using a symbol in the D_c column of Table 1. The size of each point and the thickness of its associated error bar have been scaled based on the year of publication, as indicated towards the lower left. The redshifts shown here have been dithered slightly at $z = 0.32$, $z = 0.51$, and $z = 2.33$ to make the points more clearly visible. The point at ($z = 2.33$, $\alpha_{\perp} = 0.9902$) with an overlaid black cross is a reanalysis of both the more recent and older observations at a similar z , so we show the latter with grey error bars.

Our results in Figure 1 show that all of the void models provide a better match to the observations than the homogeneous *Planck* cosmology – we will quantify this later (Section 3.1). The vast majority of the observations lie at $\alpha_{\perp} < 1$, which is not expected if the latent value is 1 and deviations arise only from random observational errors. More recent and older observations are in good agreement, as can be seen by comparing symbols with different sizes. Results from different surveys are also in good agreement, as can be seen from comparing symbols with different colours. In particular, more recent results from the Sloan Digital Sky Survey (SDSS; SDSS Collaboration 2000) also generally prefer $\alpha_{\perp} < 1$. This is in line with similar hints from the DESI results (Wang et al. 2024). It is difficult to obtain BAO results at $z \lesssim 0.3$ where a local void would have the greatest impact due to the large angular size of the BAO feature. Even so, the single available D_c measurement in this crucial regime is much more in line with the local void models than with the void-free model.

We next present results on D_H , which is inversely related to the redshift depth Δz of the BAO ruler (Equation 4). Our results are shown in Figure 2 in terms of the parameter α_{\parallel} (Equation 9). There is again a small uncertainty in the Λ CDM expectation because the CMB observations are not perfect. The void models predict that α_{\parallel} deviates from unity much less than does α_{\perp} . This is because the extra redshift due to a local void necessarily reduces the comoving distance to any fixed redshift, thereby reducing D_c . The situation with D_H is more complicated because it depends on the gradient of the outward peculiar velocity (Section 2.2.2). This is more apparent if considering the dashed lines in Figure 2, which omit the GR contribution. Without this, the models actually predict α_{\parallel} values

above unity at $z \gtrsim 0.15$. This reversed behaviour arises because the outward peculiar velocity from a local void must start declining at some point, reversing the impact on the redshift gradient. BAO observations are generally so distant that they only probe this declining region. Once the GR contribution is included, the Exponential and Gaussian profiles predict $\alpha_{\parallel} < 1$ but to a much smaller extent, while the Maxwell-Boltzmann profile predicts $\alpha_{\parallel} > 1$ across a wide range of redshifts.

Many of the observations in this redshift range do indeed show $\alpha_{\parallel} > 1$, though these are quite old. More recent measurements scatter on both sides of the model prediction by much larger amounts than any deviations predicted in the void models. Measuring Δz appears to be considerably harder than measuring $\Delta\theta$, no doubt because Δz requires fairly accurate redshifts while $\Delta\theta$ requires accurate angular positions on the sky, which are vastly easier to obtain. As a result, there are fewer α_{\parallel} measurements and these are less accurate. Importantly for testing a local solution to the Hubble tension, we could not find published D_H measurements at $z < 0.3$. Even so, it is still possible to test the prediction that deviations from unity should be much smaller for α_{\parallel} than for α_{\perp} . This is broadly in line with the observations, which scatter around unity rather than systematically going below unity, as do the α_{\perp} values in Figure 1. Partly because of the smaller predicted deviations but also because of observational difficulties, we conclude that measurements of α_{\parallel} are presently unable to distinguish between the local void models considered here and the homogeneous *Planck* cosmology.

So far, we have assumed that there is only a very small 0.2% uncertainty in r_d based on section 5.4 of Planck Collaboration VI (2020). However, the Hubble tension has motivated some workers

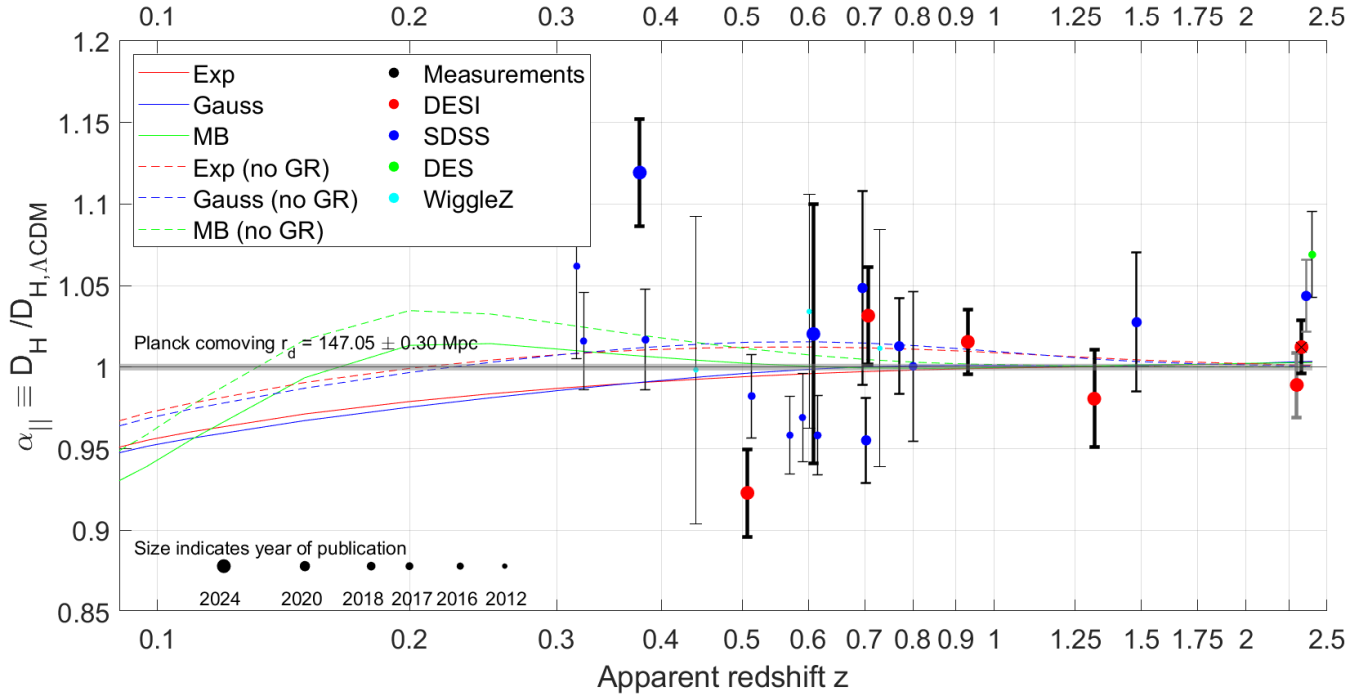


Figure 2. The ratio α_{\parallel} (Equation 9) of the Hubble distance D_H to the Λ CDM expectation at the same redshift as a function of the apparent redshift z , both according to the model (solid lines) and observations (points with uncertainties). Different void profiles are shown in different colours, as indicated in the legend. The dashed lines show results neglecting GR (Equation 1). The observations shown here are indicated using a symbol in the D_H column of Table 1. The size of each point and the thickness of its associated error bar have been scaled based on the year of publication, as indicated towards the lower left. The redshifts shown here have been dithered slightly at $z = 0.32$, $z = 0.51$, and $z = 2.33$ to make the points more clearly visible. The point at $(z = 2.33, \alpha_{\parallel} = 1.0134)$ with an overlaid black cross is a reanalysis of both the more recent and older observations at a similar z , so we show the latter with grey error bars.

to consider new physics that significantly affects the universe prior to recombination, causing large adjustments to what value of r_d is required to fit the CMB anisotropies (e.g. Poulin et al. 2019, 2023, and references therein). Since we defined α_{\parallel} and α_{\perp} with respect to the standard value of r_d , a different value would imply that these α parameters should differ from unity, albeit by a constant factor at all $z \lesssim 1000$. Much of the evidence in Figure 1 for deviations from a void-free model would be lost if such a model predicts a flat horizontal line with arbitrary rather than fixed normalisation.

This motivates us to present results in a way that is not sensitive to the assumed value of r_d . We do so using α_{AP} , which cancels out the impact of r_d by taking the ratio of parameters which depend on r_d in the same way (Equation 10). We use Figure 3 to compare observed and predicted values of α_{AP} . While this is a good idea in principle, we see that taking the ratio of quantities which are already somewhat uncertain further inflates the uncertainties. Moreover, the need for both D_c and D_H measurements from the same survey at the same z limits the number of available measurements, especially at low z . It is thus not presently possible to assess if the local void models perform better against the void-free model based on the AP parameter. In the future, measurements of α_{AP} at percent level precision in the critical $z \lesssim 0.3$ regime could be of vital importance to distinguishing if the Hubble tension should be solved through new physics in the early universe or at late times/locally.

Measurement uncertainties can be reduced by averaging different measurements rather than taking their ratio. For this purpose, we consider the isotropically averaged BAO distance D_V , which is essentially the geometric mean of D_c and D_H , albeit with the former counted twice (Equation 11). We present our results in Figure 4 in terms of the parameter α_o , which measures deviations from the

Λ CDM expectation (Equation 12). If D_c and D_H are measured independently and have the same fractional uncertainty, we would expect the fractional uncertainty on D_V to be smaller by a factor of $\sqrt{5/9}$, so we might expect typical uncertainties to be smaller by about 25% (Equation 13).

It is immediately apparent from Figure 4 that not only are the measurements indeed much more accurate, there are also many more of them. This is because D_V can be found by fitting an ellipse to the galaxy/quasar correlation function plotted against both angular separation and redshift depth. In situations where the data are too noisy to permit measuring either the width or the height of this ellipse, it might still be possible to obtain a good estimate of its area. This is why many of the BAO measurements in our compilation only give D_V , especially at very low z (Table 1). For all these reasons, the α_o parameter should provide the clearest indication of the viability of the local void solution to the Hubble tension.

The results in Figure 4 are clearly much more in line with any of the considered void models than with the void-free model. There appear to be two points at $z = 0.12 - 0.15$ that are not in line with this trend, but the uncertainty of the $z = 0.15$ point is shown in grey to indicate that it relies on data that was later reused in the $z = 0.122$ point (the same applies to the point at $z = 0.097$). As a result, the only obvious discrepancy from the local void models is the single point at $z = 0.122$, though the discrepancy is still only $2.9\sigma - 3.1\sigma$ depending on the density profile. Even with the correct model, it is plausible at the 10% level that there should be a point with this level of tension out of the 41 available D_V measurements, even before considering other issues like systematic errors or non-Gaussian tails. Still, it is clear that this particular point fits much better (0.95σ tension) with the void-free model.

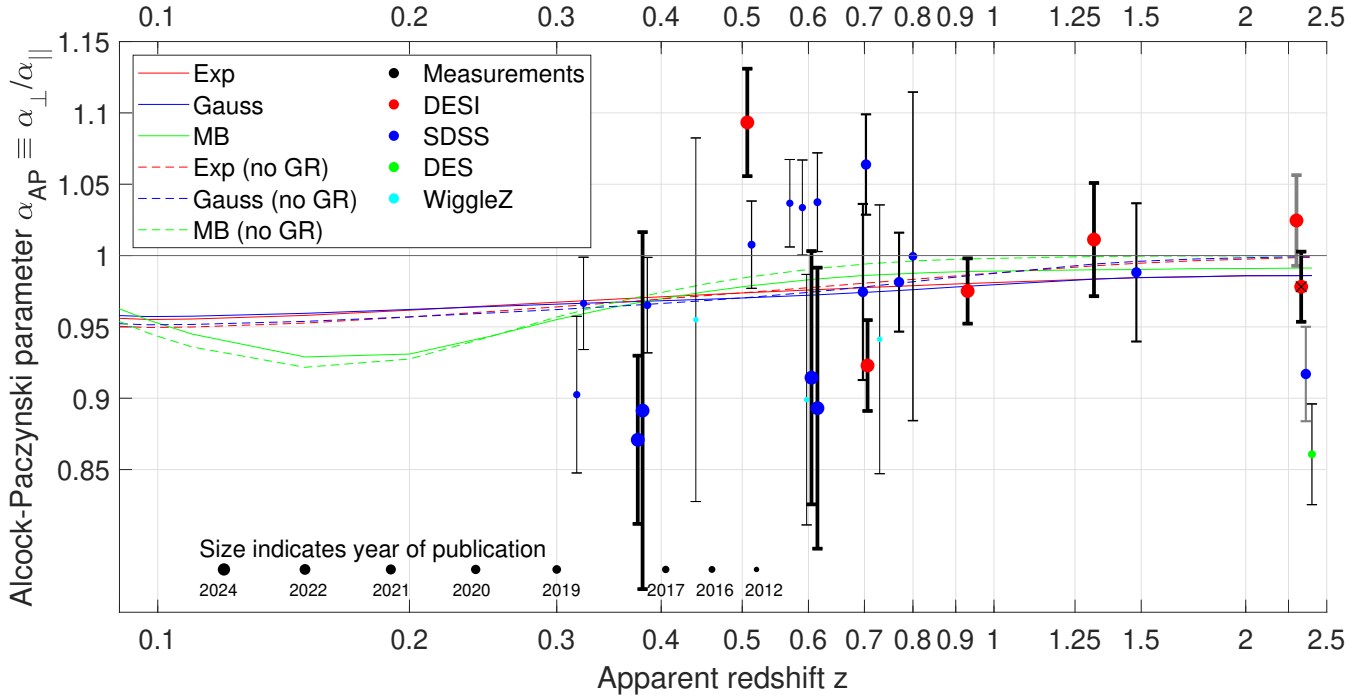


Figure 3. The AP parameter (Equation 10) as a function of the apparent redshift z according to the model (solid lines) and observations (points with uncertainties). Different void profiles are shown in different colours, as indicated in the legend. The dashed lines show results neglecting the gravitational redshift. The observations shown here are indicated using a symbol in the α_{AP} column of Table 1. We calculated α_{AP} in all cases. The size of each point and the thickness of its associated error bar have been scaled based on the year of publication, as indicated towards the lower left. The redshifts shown here have been dithered slightly at $z = 0.32$, $z = 0.51$, and $z = 2.33$ to make the points more clearly visible. The point at ($z = 2.33$, $\alpha_{\text{AP}} = 0.9771$) with an overlaid black cross is a reanalysis of both the more recent and older observations at a similar z , so we show the latter with grey error bars.

Given the importance of data at low z , we briefly mention a somewhat uncertain BAO measurement at $z = 0.07$ from an individual BAO called Ho’oleilana (Tully et al. 2023b). While the BAO scale usually has to be found through careful statistical analysis of many galaxies, a bump in the power spectrum at a particular scale makes it more likely that a large structure of galaxies will have this scale rather than a slightly smaller or larger scale. As a result, the size of the galaxy “bubble” identified by those authors can be used as a low precision constraint on the BAO scale at its redshift. Given the difficulties, the authors were inevitably only able to constrain α_o . Comparison with mock data indicates that typically it would have an uncertainty of 0.14, but we are fortunate to be living near a particularly strong and thus clearly defined individual BAO, reducing the uncertainties somewhat. As a result, observations of Ho’oleilana imply that $\alpha_o = 0.88^{+0.06}_{-0.09}$ (Tully et al. 2023b). This is in excellent ($< 1\sigma$) agreement with any of the considered void models, but 2σ below the expectation of unity in the void-free model. While one should not read too much into an individual association of galaxies, Ho’oleilana is one of several BAO observations at low z that are more in line with the considered void models. This includes the lowest z measurement of D_c shown in Figure 1, which lacks a counterpart on Figure 4.

3.1 Overall goodness of fit

We construct an approximate χ^2 statistic to assess the overall performance of each model against the observations listed in Table 1. Because of the severe complications associated with estimating covariances, we simply assume that these observations are all independent. We try to avoid double-counting data by not considering

the points shown there in grey, which are based on data that was later reanalysed and used as part of a different BAO measurement. We also exclude the somewhat speculative data point based on Ho’oleilana. In some cases, results are available from the same study with coarser or finer redshift bins. To avoid crowding the figures, we plot the former, but we use the latter when calculating χ^2 to benefit from a larger number of data points and a wider redshift range.

When considering the parameters α_{\perp} , α_{\parallel} , and α_o , we also need to make an allowance for uncertainty in the *Planck* value of r_d (147.05 ± 0.30 cMpc; see section 5.4 of Planck Collaboration VI 2020). For this, we combine in quadrature the fractional uncertainty in the *Planck* r_d with that on the corresponding α parameter, yielding a revised fractional uncertainty on the latter.

$$\frac{\sigma(\alpha)}{\alpha} \rightarrow \sqrt{\left[\frac{\sigma(\alpha)}{\alpha}\right]^2 + \left[\frac{\sigma(r_d)}{r_d}\right]^2}. \quad (14)$$

In this way, we obtain a slightly inflated $\sigma(\alpha)$, which we then use as the error budget when calculating the contribution to χ^2 . We do not apply the above procedure to the AP parameter because it is defined so that r_d cancels out (Equation 10) – only the observational uncertainty of α_{AP} is relevant.

The χ^2 values obtained in this way are shown in Table 2. Different rows show different models, while different columns show different BAO observables and combinations thereof. The number of data points (N) is indicated in the bottom row. The numbers outside brackets give the χ^2 , while the bracketed numbers immediately below them show the likelihood of a higher χ^2 for N degrees of freedom, which we express as an equivalent number of standard deviations for a single Gaussian random variable (the relation between

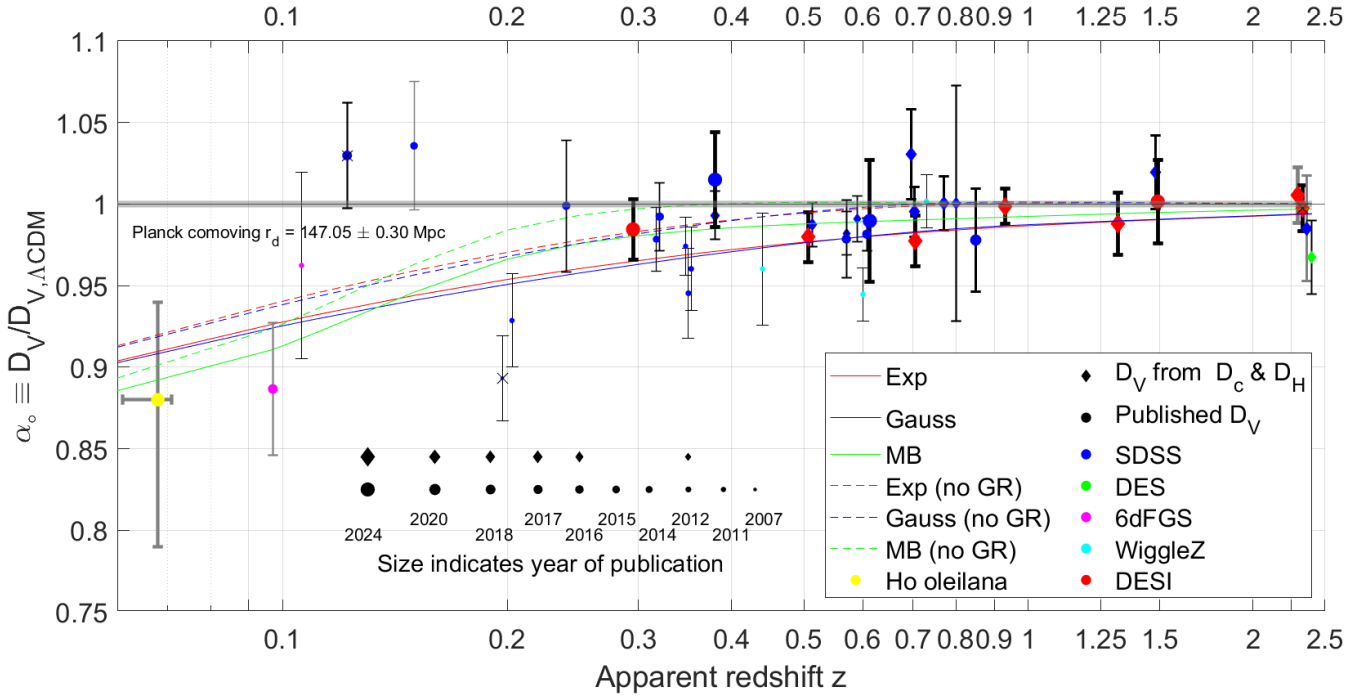


Figure 4. The ratio α_0 (Equation 12) of the isotropically averaged comoving BAO scale D_V to the Λ CDM expectation as a function of the apparent redshift z , both according to the model (solid lines) and observations (points with uncertainties). Different void profiles are shown in different colours, as indicated in the legend. The dashed lines show results neglecting GR (Equation 1). The observations shown here are indicated using a symbol in the D_V column of Table 1. The size of each point and the thickness of its associated error bar have been scaled based on the year of publication, as indicated towards the lower left. Diamond symbols indicate that we calculated D_V from the published D_c and D_H . The redshifts shown here have been dithered slightly at $z = 0.2$, $z = 0.51$, and $z = 2.33$ to make the points more clearly visible. The points at $(z = 0.122, \alpha_0 = 1.0298)$, $(z = 0.2, \alpha_0 = 0.8932)$, and $(z = 2.33, \alpha_0 = 0.9974)$ with an overlaid black cross are reanalyses of both the more recent and older observations at a similar z , so we show the latter with grey error bars. The older data used in the point at $z = 0.2$ are not shown here. The lowest redshift point at $z = 0.068$ is shown with grey uncertainties as it represents a single structure (see the text).

this ‘Z-score’ and the probability is shown in figure 2 of Asencio et al. 2023). Since BAO observations were not used in fixing the parameters of either the *Planck* cosmology or the local void models considered by HBK20, the number of degrees of freedom is the same as the number of data points, all of which can be used to test the model predictions.

Our results indicate that the void-free model is in greatest tension with all considered BAO observables and combinations thereof. The tension of $\lesssim 1.7\sigma$ is however not significant for D_c and D_H , and in any case the void models only slightly reduce it. Taking the ratio of D_c and D_H via the AP parameter (Equation 10) eliminates dependence on r_d , but it also inflates the uncertainties. All models are in moderate ($2.8\sigma - 3.0\sigma$) tension with the observed values of α_{AP} . The greatest tension again arises with the void-free model, but the void models only slightly reduce the tension. Since we worked out α_{AP} in all cases assuming independent errors on D_c and D_H , the moderate tension faced by all considered models may indicate that the uncertainties on D_c and D_H are in fact correlated to some extent, causing us to underestimate the uncertainty on α_{AP} . This suggests that we might get more accurate results not by taking the ratio of D_c and D_H but instead by taking their product, which is essentially what D_V represents (Equation 11). There are also more available measurements of α_0 than for any other α parameter. This includes several measurements at very low z , which is particularly crucial when testing the local void scenario.

The final column of Table 2 shows that the void-free control model faces 3.0σ tension with respect to α_0 , but this drops to only

Table 2. The numbers outside brackets show the χ^2 of the homogeneous *Planck* cosmology and our local void models (different rows) against different BAO observables (different columns). Results are based on the observations listed in Table 1, which we assume are all independent. We only consider the points shown there in black to avoid double-counting (see the text). The numbers in brackets show the χ^2 value as an equivalent level of tension for a single Gaussian variable, assuming the number of data points in the final row is the number of degrees of freedom. This is justified because none of the models considered here were calibrated using BAO data, which therefore serve as an independent test in all cases.

Void profile	BAO observable used to calculate χ^2			
	$\alpha_{\perp} (D_c)$	$\alpha_{\parallel} (D_H)$	α_{AP}	$\alpha_0 (D_V)$
Λ CDM	45.62	35.84	52.04	70.51
(no void)	(1.71 σ)	(1.56 σ)	(3.01 σ)	(2.99 σ)
Exponential	41.69	34.60	49.94	45.64
	(1.37 σ)	(1.44 σ)	(2.83 σ)	(1.07 σ)
Gaussian	43.92	35.53	51.44	46.70
	(1.56 σ)	(1.53 σ)	(2.96 σ)	(1.15 σ)
Maxwell-Boltzmann	31.44	34.95	49.10	44.81
	(0.53 σ)	(1.48 σ)	(2.76 σ)	(1.00 σ)
Data points	34	27	27	41

$1.0\sigma - 1.2\sigma$ when considering the void models (depending on the adopted density profile). This is because χ^2 decreases from 71 with no void to 45 – 47 in the void models, which are thus able to reduce χ^2 by about 25. A direct comparison between the homogeneous model and any of the considered void models prefers the latter

by a likelihood ratio similar to that between a model which is 5σ discrepant from an observation with Gaussian errors and a different model that exactly matches the observation. Our results therefore support the local void scenario for the Hubble tension.

The Maxwell-Boltzmann profile generally achieves a better fit to the data compared to the other void profiles, though its performance is very slightly worse than that of the Exponential profile when considering D_H . In the case of D_V (which we consider most informative due to the larger amount of data and smaller uncertainties), differences between the different void profiles are very minor, and certainly much less significant than the difference between any of the void models and the homogeneous model. The only major difference between the Maxwell-Boltzmann profile and the other void profiles arises when considering D_c , in which case it is able to reduce χ^2 by 10 – 12 compared to the other profiles. This indicates some preference for the Maxwell-Boltzmann profile, but there are also strong arguments against it based on the bulk flow curve (Mazurenko et al. 2024). Comparing the Exponential and Gaussian profiles, the former consistently achieves a lower χ^2 by 0.9 – 2.2, a negligible difference. Our results thus shed little light on which of these should be preferred.

4 DISCUSSION

Following equation 4 of Mazurenko, Banik & Kroupa (2025), the Hubble tension can be summarised as the statement that locally,

$$cz' = (1.083 \pm 0.017) H_0^{\text{Planck}}. \quad (15)$$

There is now increasingly strong evidence for the Hubble tension (Section 1; see also Uddin et al. 2024). Given the excellent fit to the CMB anisotropies in Λ CDM with the *Planck* parameters (Planck Collaboration VI 2020; Tristram et al. 2024) and that the Hubble tension is largely a mismatch between the local cz' and the present \dot{a} estimated in other ways (Perivolaropoulos 2024), the Hubble tension might indicate new physics at late times. This could be due to a local inhomogeneity, or it could indicate an adjustment to the background expansion history at late times. The latter possibility would allow us to continue making the usual assumption that $cz' = \dot{a}$, which must be the case if the universe is homogeneous on the relevant scales (see equation 3 of Mazurenko, Banik & Kroupa 2025). In either scenario, the expansion history would have followed the *Planck* cosmology for the vast majority of cosmic history. However, there would be an unexpected effect at low z that reduces the distance to any fixed z by about 10%. Roughly speaking, we would expect this to reduce the BAO distance measures by about 10% compared to the predictions of the homogeneous *Planck* cosmology. Our results in Figure 4 hint at just this kind of deviation in D_V , for which the quality and quantity of observations are better than with other common ways of presenting BAO results. While this could be a coincidence, it is at the least very interesting that BAO distance measures seem to deviate from expectations in the homogeneous *Planck* cosmology in just the way that might be expected if the Hubble tension is genuine and arises at late times.

Our focus in this contribution is on the local void scenario (HBK20). A local underdensity was originally proposed long before the Hubble tension based on galaxy number counts in the optical (Maddox et al. 1990; Shanks 1990) and especially in the near-infrared (Keenan, Barger & Cowie 2013). Based on the results of the latter study, HBK20 estimated in their equation 5 that the apparent local expansion rate (cz') should exceed H_0^{Planck} by $11 \pm 2\%$. HBK20 then constructed a semi-analytic model for the

formation of a local void from a small initial density fluctuation at high redshift. The void parameters were mostly constrained using the local cz' and the density profile of the KBC void, though the peculiar velocity of the Local Group (LG) and strong lensing time delays also played a role. Importantly, HBK20 did not consider BAO data when fitting their model parameters. Since we use the best-fitting void parameters from HBK20, our predictions for the BAO observables can be considered *a priori* predictions of the local void scenario. In this respect, it is very encouraging for this scenario that depending on the void density profile and assuming that different BAO observations are independent, there is a preference for the void model by $\Delta\chi^2 = 24 - 26$ in terms of D_V (Table 2), implying the void models are more likely than the void-free model by a factor of $\exp(\Delta\chi^2/2) > 10^5$. Given the number of data points, the overall tension drops from 3.0σ without a void to $1.0\sigma - 1.2\sigma$ in the void model, depending on the assumed initial density profile. The preference is weaker with other distance measures like D_c and D_H , though the number of available observations and their quality are both lower in these cases. Even so, the lowest χ^2 always arises with one or other void model, never with the void-free model. While it would be helpful to cancel out the dependence on r_d through use of the AP parameter, it appears that BAO results are presently not well suited to such an analysis – though this could be promising longer term.

Although the trend for BAO results to deviate from expectations in the homogeneous *Planck* cosmology particularly at low z supports the local void scenario, they do not uniquely imply its validity. This is because the results might instead be due to a homogeneous cosmology whose expansion history deviates from the *Planck* cosmology at late times. Such deviations could be due to evolution of the dark energy density, for instance in the cascading dark energy (CDE) scenario (Rezazadeh, Ashoorioon & Grin 2024). Additional observations at low z would be required to distinguish such late-time background solutions from a local void. In this regard, we note that Huang, Wang & Yu (2025) claimed to find “strong evidence against homogeneous new physics over Λ CDM” based on a compilation of SNe, BAO, and cosmic chronometer (CC) data, with the authors suggesting instead that the solution lies with “local-scale inhomogeneous new physics disguised as local observational systematics”. Moreover, a slightly modified expansion history with standard growth of structure on $\gtrsim 100$ Mpc scales would not explain the observed size and depth of the KBC void, whose properties are in 6.0σ tension with Λ CDM expectations (HBK20). Nor would it explain the anomalously fast observed bulk flows (Watkins et al. 2023; Whitford et al. 2023). Additional evidence for enhanced growth of structure is provided by the high redshift, mass, and collision velocity of the interacting galaxy clusters known as El Gordo (Menanteau et al. 2012), whose properties are incompatible with Λ CDM at $> 5\sigma$ confidence for any plausible collision velocity (Asencio, Banik & Kroupa 2021, 2023). Giant arcs and rings of quasar absorbers may also be in tension with Λ CDM (Lopez, Clowes & Williger 2022, 2024), though a more detailed comparison with Λ CDM expectations is required to account for the biased nature of the tracers. This issue is not important in the galaxy number counts of Keenan, Barger & Cowie (2013) because their survey covers most (57 – 75%) of the galaxy luminosity function over 90% of the sky (see their figure 9b).

To some extent, the tension between BAO observables and the homogeneous *Planck* cosmology could be addressed by altering r_d , which would require new physics prior to recombination. BAO observations at high z impose strong constraints on the extent

to which this is possible. For instance, the highest redshift DESI measurement of D_V/r_d at $z = 2.33$ including reanalysis of earlier results (the crossed red point on Figure 4) implies that any change should be $\lesssim 1\%$. This is part of a wider problem: the BAO results suggest a trend in α_\circ with z , not a fixed offset from unity at all z . Additional BAO observations at $z \lesssim 0.3$ will be crucial to assessing the significance of this trend and the similar trend in α_\perp (Figure 1).

While our results seem to favour a late-time or local solution to the Hubble tension, it is worth discussing solutions at early times, especially through new physics prior to recombination that allow the CMB anisotropies to be fit with higher H_0 . An important consequence of such models is that the expansion history would closely follow the *Planck* cosmology for the vast majority of cosmic history ($z \lesssim 1000$), but with a compressed timeline due to the higher H_0 . It is possible to test this using the ages of the oldest Galactic stars (Cimatti & Moresco 2023). Allowing a modest amount of time between the Big Bang and the formation of the considered stars, the resulting H_0 value is shown using a magenta band on figure 3 of Mazurenko, Banik & Kroupa (2025). It is clear that H_0 obtained in this way is much more in line with H_0^{Planck} than the local cz' . This is because the Universe has an age similar to that in the *Planck* cosmology, so reducing the predicted age by almost a Gyr leads to many stellar ages exceeding the revised cosmic age (see also Xiang et al. 2024).

The above result is based on the absolute ages of stars, but it is possible to use instead differential ages in the CC technique (Jimenez & Loeb 2002; Moresco et al. 2018, 2020; Moresco 2024). The chronometers in this case are massive quiescent galaxies that stopped forming stars at early times. Detailed analysis of their spectra gives an idea of their age, which can be compared between populations at different z to get the elapsed time. In this way, it is possible to obtain the slope of the time-redshift relation. Results from this technique in combination with other uncalibrated datasets (which cannot constrain H_0 on their own) give H_0 values very close to H_0^{Planck} (Cogato et al. 2024; Guo et al. 2024). Moreover, the latter authors found that the inferred H_0 is $> 4\sigma$ below the local cz' .

Early-time solutions to the Hubble tension might also face difficulties fitting the CMB anisotropies. Since uncalibrated BAO results tightly constrain Ω_M to very near the *Planck* value (Lin, Chen & Mack 2021), higher H_0 implies a higher matter density as the critical density $\propto H_0^2$, but the observed CMB temperature tightly constrains the radiation energy density regardless of H_0 . Thus, models with a higher H_0 and no new physics at $z \lesssim 1000$ would have a different ratio between the matter and radiation densities at recombination. This would alter the pattern of acoustic oscillations in the CMB power spectrum, requiring careful fine-tuning to retain a similarly good fit. There might also be an impact on the epoch of matter-radiation equality, changing the turnover scale in the matter power spectrum (Eisenstein & Hu 1998). However, the observed matter power spectrum favours $H_0 = H_0^{\text{Planck}}$ (Philcox et al. 2022; Farren et al. 2024). These and other problems with early-time solutions to the Hubble tension were reviewed in Vagnozzi (2023), which focused on seven main issues. A late-time solution would have minimal effect on many of these issues, e.g. CC results require a long time baseline and are barely sensitive to $z \lesssim 0.3$, a revised expansion history only in the last few Gyr would hardly affect the cosmic age or the angular diameter distance to the surface of last scattering, and the horizon size at matter-radiation equality should not be affected given this occurs when the universe is $7\times$ younger than at recombination (Banik & Samaras 2024).

Another important clue is that the Hubble tension seems to become weaker at high redshift, and not merely due to larger uncer-

ainties (Bousis & Perivolaropoulos 2024). The redshift dependence of the Hubble tension was explored in some detail by Mazurenko, Banik & Kroupa (2025) using the concept of $H_0(z)$, the value of H_0 that would be inferred by observers using data in a narrow redshift range centred on z . Using three methods to estimate how observers might go about extrapolating high redshift results to obtain the present expansion rate, those authors predicted $H_0(z)$ using the local void models considered by HBK20, again restricting to their best-fitting parameters for each of the three density profiles they considered. In this way, Mazurenko, Banik & Kroupa (2025) found quite good agreement with recent observational results (Jia et al. 2023, 2025). In particular, the void models predict a curve that goes approximately halfway between the observational results of these two studies (see figure 3 of Mazurenko, Banik & Kroupa 2025). An early-time solution to the Hubble tension should lead to a flat $H_0(z)$ curve at the level of the local cz' . However, a descending trend is detected at 5.6σ significance (Jia, Hu & Wang 2023), rising to 6.4σ upon including the DESI BAO results (Jia et al. 2025). Their empirical $H_0(z)$ curve declines from the local cz' and becomes approximately flat at H_0^{Planck} for $z \gtrsim 0.6$, suggesting that the background expansion history was following the *Planck* cosmology until fairly recently.

5 CONCLUSIONS

Redshifts increase more rapidly with distance than expected in the Λ CDM cosmological paradigm if its parameters are calibrated to fit the CMB anisotropies. This Hubble tension might arise from outflows driven by a local supervoid, which interestingly is suggested by source number counts across the whole electromagnetic spectrum (see section 1.1 of HBK20, and references therein). Those authors constructed a semi-analytic model for the formation of the KBC void out of a small initial density fluctuation at high redshift. They obtained best-fitting parameters for three different density profiles (Exponential, Gaussian, and Maxwell-Boltzmann) by considering the fit to various observables, the main ones being the local redshift gradient and the observed density profile of the KBC void.

In this contribution, we explore the consequences of these models for BAO datasets, which were not considered by HBK20. After briefly recapping how the BAO observables should be calculated in a homogeneously expanding cosmology (Section 2.1), we explain how a local void distorts the relation between these observables and the redshift (Section 2.2). We then compile a list of BAO observations from the past twenty years (Table 1). We use this to test the performance of the local void models and a control void-free model that assumes the homogeneous *Planck* cosmology.

Our results show that D_H and the AP parameter are presently not very discriminative, partly because of observational difficulties, but also because of various effects in the void model cancelling each other out and thereby reducing the expected deviations from the void-free model. Results based on D_c fit somewhat better in the local void models (Figure 1). We found that the most discriminative quantity is the isotropically averaged BAO distance D_V , whose ratio with expectations in the control model is shown in Figure 4 as a function of z . The results generally conform much more closely to the void models than the void-free model, apart from a single data point that is discrepant by close to 3σ but in just under 1σ tension with the control model.

We use an approximate χ^2 statistic to estimate the overall goodness of fit of each model to our compilation of BAO observations, removing duplicates where a study reuses data that underpinned an

earlier study. The χ^2 values obtained in this way are summarised in Table 2, which shows that the void-free model provides the worst fit in all cases. Focusing on D_V due to the larger number of available measurements and their smaller uncertainties, we see that the void-free model has $\chi^2 = 71$, which implies 3.0σ tension for 41 data points. The void models can reduce this to 45–47 depending on the density profile, even though the parameters in each case were fixed by HBK20 without considering BAO datasets. The preference for the void models by $\Delta\chi^2 = 24 - 26$ implies that they are more likely than the void-free model by a factor of $\exp(\Delta\chi^2/2) > 10^5$ when considering only the D_V data. The preference is weaker in other common ways of presenting BAO results (Table 2). We are unable to shed much light on which of the void models performs best. We note that there are arguments against the Maxwell-Boltzmann profile based on the bulk flow curve at $z < 0.083$ (Mazurenko et al. 2024), despite its somewhat better fit to the BAO data compared to the other profiles.

Our work highlights the importance of BAO observations at $z \lesssim 0.3$ in testing local solutions to the Hubble tension. These observations are challenging due to the large angular size of the BAO ruler, but they are particularly crucial. There is a trade-off between the redshift and the accuracy required to test the local void model, which predicts the largest deviations at low z . Our predictions can give observers an idea of how to weigh the scientific return of a more accurate BAO measurement at higher z compared to a less accurate measurement at lower z . They can also provide guidance on which types of BAO measurements to prioritise, since the expected signal is not the same for angular and line of sight measures (D_c and D_H , respectively). Longer term improvements to the accuracy and redshift coverage will allow the AP test, making the results immune to the assumed value of r_d (Section 2.2.3).

A local void was proposed long before the Hubble tension based on galaxy number counts in the optical (Maddox et al. 1990; Shanks 1990) and especially in the near-infrared (Keenan, Barger & Cowie 2013). Outflow from the KBC void can solve the Hubble tension in the semi-analytic models of HBK20, who calibrated their model parameters without considering BAO data. As a result, the predictions of their model for the BAO observables must be considered *a priori* predictions. Our results show that these predictions are fairly successful, in all cases achieving a better fit than the homogeneous *Planck* cosmology (Table 2). This is especially true when considering D_V , for which the quantity and quality of available data are both superior to other common ways of presenting BAO data. We therefore plan to further test the local void scenario by exploring the local velocity field in more detail (Stiskalek et al., in preparation). This will be complemented by a higher redshift test using SNe, which we plan to analyse using a novel method that allows greater flexibility in the relation between luminosity distance and redshift, thereby reducing sensitivity to the assumed cosmological model (Lane et al. 2025; Seifert et al. 2025).

ACKNOWLEDGEMENTS

IB is supported by Royal Society University Research Fellowship grant 211046 and was supported by Science and Technology Facilities Council grant ST/V000861/1. The contribution of VK was enabled by an undergraduate research bursary from the Royal Astronomical Society. For the purpose of open access, the authors have applied a Creative Commons Attribution (CC BY) licence to any Author Accepted Manuscript version arising.

DATA AVAILABILITY

Details of the void simulations were previously published in HBK20 along with the parameters of the most likely model for each void density profile. The observational BAO results used here were previously published in the cited studies. An EXCEL summary table with these measurements is available on request to the second author.

REFERENCES

- Alam S., et al., 2017, *MNRAS*, **470**, 2617
 Alcock C., Paczynski B., 1979, *Nature*, **281**, 358
 Anderson L., et al., 2014, *MNRAS*, **441**, 24
 Angulo R. E., Springel V., White S. D. M., Jenkins A., Baugh C. M., Frenk C. S., 2012, *MNRAS*, **426**, 2046
 Asencio E., Banik I., Kroupa P., 2021, *MNRAS*, **500**, 5249
 Asencio E., Banik I., Kroupa P., 2023, *ApJ*, **954**, 162
 Banik I., Samaras N., 2024, preprint, *Arxiv* (arXiv:2410.00804)
 Banik I., Zhao H., 2022, *Symmetry*, **14**, 1331
 Bennett C. L., et al., 2003, *ApJ*, **583**, 1
 Beutler F., et al., 2011, *MNRAS*, **416**, 3017
 Blake C., et al., 2011, *MNRAS*, **418**, 1707
 Blake C., et al., 2012, *MNRAS*, **425**, 405
 Böhringer H., Chon G., Bristow M., Collins C. A., 2015, *A&A*, **574**, A26
 Böhringer H., Chon G., Collins C. A., 2020, *A&A*, **633**, A19
 Bousis D., Perivolaropoulos L., 2024, *Physical Review D*, **110**, 103546
 Buswell G. S., Shanks T., Frith W. J., Outram P. J., Metcalfe N., Fong R., 2004, *MNRAS*, **354**, 991
 Camarena D., Marra V., 2018, *Physical Review D*, **98**, 023537
 Camarena D., Marra V., 2020a, *Physical Review Research*, **2**, 013028
 Camarena D., Marra V., 2020b, *MNRAS*, **495**, 2630
 Carter P., Beutler F., Percival W. J., Blake C., Koda J., Ross A. J., 2018, *MNRAS*, **481**, 2371
 Chen S. F., et al., 2024, *MNRAS*, **534**, 544
 Chuang C.-H., Wang Y., 2012, *MNRAS*, **426**, 226
 Chuang C.-H., Wang Y., Hemantha M. D. P., 2012, *MNRAS*, **423**, 1474
 Chuang C.-H., et al., 2017, *MNRAS*, **471**, 2370
 Cimatti A., Moresco M., 2023, *ApJ*, **953**, 149
 Cogato F., Moresco M., Amati L., Cimatti A., 2024, *MNRAS*, **527**, 4874
 Cole S., et al., 2005, *MNRAS*, **362**, 505
 DES & SPT Collaborations 2018, *MNRAS*, **480**, 3879
 DES Collaboration 2019, *MNRAS*, **483**, 4866
 DES Collaboration 2022, *Physical Review D*, **105**, 043512
 DES Collaboration 2024, *Physical Review D*, **110**, 063515
 DESI Collaboration 2016, preprint, *Arxiv* (arXiv:1611.00036)
 DESI Collaboration 2022, *AJ*, **164**, 207
 DESI Collaboration 2024, *JCAP*, in press
 Dahmani S., Bouali A., El Bojaddaini I., Errahmani A., Ouali T., 2023, *Physics of the Dark Universe*, **42**, 101266
 Di Valentino E., 2021, *MNRAS*, **502**, 2065
 Di Valentino E., et al., 2021, *Classical and Quantum Gravity*, **38**, 153001
 Dicke R. H., Peebles P. J. E., Roll P. G., Wilkinson D. T., 1965, *ApJ*, **142**, 414
 Efstathiou G., Sutherland W. J., Maddox S. J., 1990, *Nature*, **348**, 705
 Eisenstein D. J., Hu W., 1998, *ApJ*, **496**, 605
 Eisenstein D. J., et al., 2005, *ApJ*, **633**, 560
 Famaey B., McGaugh S. S., 2012, *Living Reviews in Relativity*, **15**, 10
 Farren G. S., et al., 2024, preprint, *Arxiv* (arXiv:2409.02109)
 Freedman W. L., Madore B. F., Jang I. S., Hoyt T. J., Lee A. J., Owens K. A., 2024, preprint, *Arxiv* (arXiv:2408.06153)
 Frith W. J., Buswell G. S., Fong R., Metcalfe N., Shanks T., 2003, *MNRAS*, **345**, 1049
 Frith W. J., Shanks T., Outram P. J., 2005, *MNRAS*, **361**, 701
 Frith W. J., Metcalfe N., Shanks T., 2006, *MNRAS*, **371**, 1601
 Giare \bar{W} ., Najafi M., Pan S., Di Valentino E., Firouzjaee J. T., 2024, *JCAP*, **2024**, 035
 Gil-Marín H., et al., 2020, *MNRAS*, **498**, 2492

- Gómez-Valent A., Favale A., Migliaccio M., Sen A. A., 2024, *Physical Review D*, **109**, 023525
- Guo W., et al., 2024, preprint, [Arxiv \(arXiv:2412.13045\)](#)
- Harko T., 2023, *Physical review D*, **107**, 123507
- Haslbauer M., Banik I., Kroupa P., 2020, *MNRAS*, **499**, 2845
- Hinshaw G., et al., 2003, *ApJS*, **148**, 135
- Hou J., et al., 2021, *MNRAS*, **500**, 1201
- Huang J. S., Cowie L. L., Gardner J. P., Hu E. M., Songaila A., Wainscoat R. J. 1997, *ApJ*, **476**, 12
- Huang L., Wang S.-J., Yu W.-W., 2025, *Science China Physics, Mechanics, and Astronomy*, **68**, 220413
- Ivanov M. M., Simonović M., Zaldarriaga M., 2020, *JCAP*, **2020**, 042
- Jia X. D., Hu J. P., Wang F. Y., 2023, *A&A*, **674**, A45
- Jia X. D., Hu J. P., Yi S. X., Wang F. Y., 2025, *ApJL*, in press
- Jimenez R., Loeb A., 2002, *ApJ*, **573**, 37
- Keenan R. C., Barger A. J., Cowie L. L., 2013, *ApJ*, **775**, 62
- Komatsu E., et al., 2009, *ApJS*, **180**, 330
- Kroupa P., 2015, *Canadian Journal of Physics*, **93**, 169
- Lane Z. G., Seifert A., Ridden-Harper R., Wiltshire D. L., 2025, *MNRAS*, **536**, 1752
- Lin W., Chen X., Mack K. J., 2021, *ApJ*, **920**, 159
- Lopez A. M., Clowes R. G., Williger G. M., 2022, *MNRAS*, **516**, 1557
- Lopez A. M., Clowes R. G., Williger G. M., 2024, *JCAP*, **2024**, 055
- Ludwick K. J., 2017, *Modern Physics Letters A*, **32**, 1730025
- Maddox S. J., Efstathiou G., Sutherland W. J., Loveday J., 1990, *MNRAS*, **242**, 43
- Mazurenko S., Banik I., Kroupa P., Haslbauer M., 2024, *MNRAS*, **527**, 4388
- Mazurenko S., Banik I., Kroupa P., 2025, *MNRAS*, **536**, 3232
- Menanteau F., et al., 2012, *ApJ*, **748**, 7
- Milgrom M., 1983, *ApJ*, **270**, 365
- Moresco M., 2024, preprint, [Arxiv \(arXiv:2412.01994\)](#)
- Moresco M., Jimenez R., Verde L., Pozzetti L., Cimatti A., Citro A., 2018, *ApJ*, **868**, 84
- Moresco M., Jimenez R., Verde L., Cimatti A., Pozzetti L., 2020, *ApJ*, **898**, 82
- Neveux R., et al., 2020, *MNRAS*, **499**, 210
- Nusser A., 2016, *MNRAS*, **455**, 178
- Ostriker J. P., Steinhardt P. J., 1995, *Nature*, **377**, 600
- Peery S., Watkins R., Feldman H. A., 2018, *MNRAS*, **481**, 1368
- Penzias A. A., Wilson R. W., 1965, *ApJ*, **142**, 419
- Percival W. J., Cole S., Eisenstein D. J., Nichol R. C., Peacock J. A., Pope A. C., Szalay A. S., 2007, *MNRAS*, **381**, 1053
- Percival W. J., et al., 2010, *MNRAS*, **401**, 2148
- Perivolaropoulos L., 2024, *Physical Review D*, **110**, 123518
- Philcox O. H. E., Farren G. S., Sherwin B. D., Baxter E. J., Brout D. J., 2022, *Physical Review D*, **106**, 063530
- Planck Collaboration VI 2020, *A&A*, **641**, A6
- Planck Collaboration XXVII 2014, *A&A*, **571**, A27
- Poulin V., Smith T. L., Karwal T., Kamionkowski M., 2019, *Physical Review Letters*, **122**, 221301
- Poulin V., Smith T. L., Karwal T., 2023, *Physics of the Dark Universe*, **42**, 101348
- Rezazadeh K., Ashoorioon A., Grin D., 2024, *ApJ*, **975**, 137
- Riess A. G., et al., 2022, *ApJ*, **938**, 36
- Riess A. G., et al., 2024, *ApJ*, **977**, 120
- Ross A. J., Samushia L., Howlett C., Percival W. J., Burden A., Manera M., 2015, *MNRAS*, **449**, 835
- Rubart M., Schwarz D. J., 2013, *A&A*, **555**, A117
- Rubart M., Bacon D., Schwarz D. J., 2014, *A&A*, **565**, A111
- SDSS Collaboration 2000, *AJ*, **120**, 1579
- Said K., et al., 2024, preprint, [Arxiv \(arXiv:2408.13842\)](#)
- Schirra A. P., Quartin M., Amendola L., 2024, preprint, [Arxiv \(arXiv:2406.15347\)](#)
- Scolnic D., Vincenzi M., 2023, preprint, [Arxiv \(arXiv:2311.16830\)](#)
- Scolnic D., et al., 2025, *ApJL*, **979**, L9
- Seifert A., Lane Z. G., Galoppo M., Ridden-Harper R., Wiltshire D. L., 2025, *MNRAS*, **537**, L55
- Seo H.-J., et al., 2012, *ApJ*, **761**, 13
- Shanks T., 1990, in Bowyer S., Leinert C., eds, *International Astronomical Union Symposium no. 139 Vol. 139, The Galactic and Extragalactic Background Radiation*. Springer Dordrecht, pp 269–281
- Slepian Z., et al., 2017, *MNRAS*, **469**, 1738
- Spergel D. N., et al., 2003, *ApJS*, **148**, 175
- Spergel D. N., et al., 2007, *ApJS*, **170**, 377
- Sridhar S., et al., 2020, *ApJ*, **904**, 69
- Tristram M., et al., 2024, *A&A*, **682**, A37
- Tully R. B., et al., 2023a, *ApJ*, **944**, 94
- Tully R. B., Howlett C., Pomarède D., 2023b, *ApJ*, **954**, 169
- Uddin S. A., et al., 2024, *ApJ*, **970**, 72
- Vagnozzi S., 2023, *Universe*, **9**, 393
- Wagenveld J. D., et al., 2024, *A&A*, **690**, A163
- Wang Y., et al., 2020, *MNRAS*, **498**, 3470
- Wang Z., Lin S., Ding Z., Hu B., 2024, *MNRAS*, **534**, 3869
- Watkins R., et al., 2023, *MNRAS*, **524**, 1885
- Whitbourn J. R., Shanks T., 2014, *MNRAS*, **437**, 2146
- Whitbourn J. R., Shanks T., 2016, *MNRAS*, **459**, 496
- Whitford A. M., Howlett C., Davis T. M., 2023, *MNRAS*, **526**, 3051
- Wong J. H. W., Shanks T., Metcalfe N., Whitbourn J. R., 2022, *MNRAS*, **511**, 5742
- Xiang M., Rix H.-W., Yang H., Liu J., Huang Y., Frankel N., 2024, *Nature Astronomy*, in press
- Yao Y.-H., Meng X.-H., 2023, *Physics of the Dark Universe*, **39**, 101165
- Zhao G.-B., et al., 2021, *MNRAS*, **504**, 33
- Zhu F., et al., 2018, *MNRAS*, **480**, 1096
- de Bernardis P., et al., 2000, *Nature*, **404**, 955
- de Carvalho E., Bernui A., Avila F., Novaes C. P., Nogueira-Cavalcante J. P., 2021, *A&A*, **649**, A20
- de Mattia A., et al., 2021, *MNRAS*, **501**, 5616
- du Mas des Bourboux H., et al., 2020, *ApJ*, **901**, 153

This paper has been typeset from a $\text{\TeX}/\text{\LaTeX}$ file prepared by the authors.